JOURNAL OF MATERIALS SCIENCE **39** (2004) 5071–5079

Mechanical alloying in binary Fe-M (M = C, B, Al, Si, Ge, Sn) systems

E. P. YELSUKOV*, G. A. DOROFEEV
Physical-Technical Institute UrB RAS, 426001 Izhevsk, Russia
E-mail: yelsukov@fnms.fti.udm.ru

The processes of mechanical alloying of iron and sp-elements (C, B, Al, Si, Ge, Sn) under identical conditions of mechanical treatment have been studied. General regularities and differences in the mechanisms and kinetics of solid state reactions have been ascertained. A microscopic model of mechanical alloying in these systems is suggested.

1. Introduction

One of the main points in studying mechanical alloying (MA) is finding out microscopic mechanisms of solid state reactions (SSRs), in particular, those of forming supersaturated solid solutions. In other words, what do we imply by the term "deformation atomic mixing"? It is also necessary to find out the major factors determining the SSRs kinetics. Appropriate model systems for such an investigation are binary powder mixtures of Fe with sp-elements (M) such as C, B, Al, Si, Ge, Sn. The ratio of the covalent radii R_M/R_{Fe} changes in a wide range from 0.66 (C) to 1.21 (Sn). The equilibrium phase diagrams of the Fe-M alloys are characterized by different types: with actual absence of solubility of the M atoms in α-Fe (Fe-C and Fe-B), with low solubility (Fe-Sn) and broad concentration range of solid solutions (Fe-Al, Fe-Si, Fe-Ge). MA in these Fe-M systems has attracted the attention of many research teams over the last 15 years. A detailed analysis of the data published is presented in our papers [1–11]. In general, one can ascertain that MA is proceeded by the formation of laminar structure with characteristic sizes of 1–10 μm (see, e.g. [12, 13]). However, detailed comparisons of the mechanisms and kinetics of MA in the Fe-M systems on the basis of the earlier published data are not possible for the following reasons:

(i) MA was carried out under different conditions: the material of grinding tools, power intensity of milling devices. The latter characteristic has not been presented as a rule;
(ii) There are considerable differences in the results published.

In the present work, we have classified the results of our investigation of the mechanisms and kinetics of MA in the Fe-M systems under equal conditions of treatment in a mill with the known power intensity and controlled levels of contamination and heating of the samples studied. The results of other authors have been taken into account as well.

2. Experimental

For MA, mixtures of pure Fe (99.99) and sp-elements (99.99) powders with particle size less than 300 μm were used. MA was carried out in an inert atmosphere (Ar) in a planetary ball mill Fritsch P-7 with a power intensity 2.0 W/g. For each given mechanical treatment time the mass of the loaded sample was 10 g. With the given power intensity the time of mechanical treatment of 1 h corresponds to the dose of 7 kJ/g. Using air forced-cooling, the heating of the vials, balls and sample did not exceed 60°C. The milling tools—vials (volume 45 cm^3) and balls (20, diameter 10 mm) were made of hardened steel containing 1 wt% C and 1.5 wt% Cr. Possible contamination of the sample by material from the milling tools was monitored by the measurement of the powder, vial and ball mass before and after treatment. X-ray diffractometer with Cu K_α monochromatized radiation was used for X-ray examinations of samples. Phase composition was determined from X-ray diffraction (XRD) patterns using Rietveld method. The crystallite size ($\langle L \rangle$) and microstrains ($\langle \varepsilon^2 \rangle^{1/2}$) were calculated from peak profile analysis using the Voigt function. Room-temperature Mössbauer investigations were carried out with a conventional constant acceleration spectrometer and ^{57}Co(Cr) source. To estimate the size of the powder particles after MA an Auger spectrometer in secondary-electron microscopy mode image was used. For all the systems studied the particles size after MA was in the range of 5–20 μm.

3. Results and discussion

3.1. Milling of pure Fe

Under the given conditions we showed in [14] that with the milling time $t_{mil} = 1$ h the grain size in α-Fe particles $\langle L \rangle = 13$ nm. On increasing the t_{mil} up to 16 h $\langle L \rangle$

*Author to whom all correspondence should be addresed.

decreases to 9 nm, and the bcc lattice parameter of α-Fe increases to 0.2869 nm. In [14] the concept of interface regions is introduced, which include the boundary and close-to-boundary distorted zones. The width of interfaces (d) can be estimated, according to [15, 16], as 1 nm. With $\langle L\rangle = 9$ nm the volume fraction of interfaces (f_{if}) is ~15%. Supposing that in the body of the grain the bcc lattice parameter is equal to 0.2866 nm, we obtain the average lattice parameter in distorted zone of interfaces 0.2887 nm, i.e. almost by 1% more than in typical α-Fe. The existence of the distorted zones is confirmed by symmetrical broadening by 20% of the lines of the Mössbauer spectrum (MS) of the milled α-Fe without emergence of any new components in the spectrum.

3.2. Mechanical alloying of Fe-C and Fe-B

Carbon and boron practically do not dissolve in α-Fe, their covalent radii are much less than that of Fe: $R_C/R_{Fe} = 0.66$ and $R_B/R_{Fe} = 0.75$. It was established [7, 8, 12, 17] that in the C concentration range $0 < x \leq 25$ at.% in the initial mixture there was a critical concentration $x = 17$ at.% at which the change of the type of SSRs in MA took place. In [5, 8] we found the following types of SSRs with $x \geq 17$ at.% C.

$$17 \leq x < 25,\ \mathrm{Fe} + \mathrm{C} \rightarrow \mathrm{Fe} + \mathrm{Am(Fe\text{-}C)} \rightarrow \mathrm{Fe} + \mathrm{Am(Fe\text{-}C)} + (\mathrm{Fe_3C})_D;$$

$$x = 25,\ \mathrm{Fe} + \mathrm{C} \rightarrow \mathrm{Fe} + \mathrm{Am(Fe\text{-}C)} \rightarrow (\mathrm{Fe_3C})_D,$$

where Am(Fe-C) designates the amorphous Fe-C phase the concentration of C in which is close to 25 at.%; $(Fe_3C)_D$ designates distorted cementite. All of these SSRs take place after reaching the nanocrystalline state in the α-Fe particles ($\langle L\rangle < 10$ nm). The estimates of the Am(Fe-C) phase amount showed [5–8] that it formed in the interfaces of the α-Fe nanostructure. The given SSRs types with $x \geq 17$ agree with the data published earlier in [12, 18, 19]. However, they differ from the results of [17, 20] in which, along with cementite, hexagonal carbides were found, and from [21, 22] in which only cementite as the first MA stage was found to be formed.

Controversial results were obtained for a single-stage process of MA as well with $x < 17$ at.% C: hexagonal carbides [17], interstitial solid solution [23] and amorphous Fe-C phase [7, 8, 11]. Consider in detail the process of MA with the C concentration in the initial mixture $x = 15$ at.% [11]. In the XRD patterns, broadened bcc reflections are revealed, which positions do not change as t_{mil} increases and correspond to those of the α-Fe lines. The grain size decreases from 100 nm for the initial powder to 6 nm at $t_{mil} = 1$ h and 3 nm at $t_{mil} = 16$ h. Besides at the base of (110) peak there is a considerable increase of intensity, which is similar to the contribution from the first peak of the amorphous phase. In the MS and hyperfine magnetic field (HFMF) distribution functions P(H) besides the component attributed to pure α-Fe (H = 330 kOe) there is a component with broad distribution of HFMF from 50 to 330 kOe. It is obvious that the given component corresponds to the Am(Fe-C) phase which produced "halo" in XRD patterns. The known concentration dependence of the average value of HFMF for amorphous Fe-C films [24] allowed us to estimate the C concentration in the Am(Fe-C) phase as equal to ~25 at.% C. The average grain size calculated from XRD patterns and the amount of the amorphous Am(Fe-C) phase (f_{Am}) in the process of MA calculated from the MS are given in Fig. 1. Comparing the dependences $f_{Am}(t_{mil})$ and $\langle L\rangle(t_{mil})$ one can draw the conclusion that SSR of the amorphous phase formation takes place on condition of nanocrystalline state realization in the α-Fe particles. The atomic fraction of the Am(Fe-C) phase increases from 0.15 ($t_{mil} = 1$ h) to 0.67 ($t_{mil} = 16$ h). To account for the amorphous phase amount, the conception on the existence of interfaces is applied. Fig. 1b gives the calculated dependence of the volume fraction of the interfaces $f_{if}(t_{mil})$ according to the obtained grain sizes (Fig. 1a), the given interface width of 1nm and on the assumption of a cubic grain shape. The comparison of the dependences $f_{Am}(t_{mil})$ and $f_{if}(t_{mil})$ illustrates not only qualitative but also quantitative agreement. It allows us to draw the conclusion on the amorphous phase formation in the interfaces of the α-Fe nanostructure. In Section 3.1. we estimated the bcc parameter of the distorted structure in the interfaces of 0.2887 nm. One can suppose that the increase of the size of the interstices in the distorted structure in comparison with that of the grain body of α-Fe ($a = 0.2866$ nm) makes the dissolution of C atoms in the interfaces easier under pulse mechanical treatment. Additional distortions during C dissolution lead to amorphization of the interfaces.

MA in the Fe-B system was studied in [25–30] with the B content in the initial mixture from 20 to 60 at.%. In [25] it was shown that with the content of B of 20 at.% MA was realized during one stage: Fe + B → Fe + Am(Fe-B). At the same time the stage of the

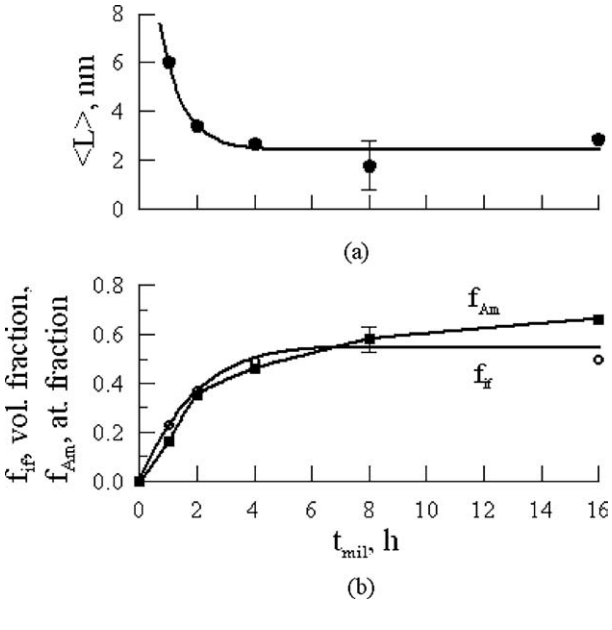

Figure 1 Time dependences of the α-Fe grain size (a), atomic fraction of amorphous phase (f_{Am}) and volume fraction of interfaces (f_{if}) (b) during MA in the Fe(85)C(15) system [11].

amorphous phase formation precedes the formation of borides with a higher amount of B [26–30]. The given data show considerable similarity in the type of SSRs in the Fe-C and Fe-B systems. However, so far, detailed investigations of the kinetics of the initial SSRs stage in MA in the Fe-B system and its comparison with that of the Fe-C system have not been carried out. With this purpose in the present paper we have chosen the content of the initial mixture as Fe(85)B(15), mechanical treatment of which was carried out under the same conditions as for the Fe(85)C(15) mixture. All the changes observed in XRD patterns and MS of the mechanically alloyed samples Fe(85)B(15) are similar to those of the Fe(85)C(15) samples. The fractions of Fe atoms in the amorphous phase found from the MS depending on t_{mil} for Fe(85)B(15) (present work) and Fe(85)C(15) [11] are given in Fig. 2a. In both systems the condition of SSRs proceeding is reaching the nanostructure state in α-Fe (Fig. 2b). However, in the Fe-C system the formation of the amorphous phase starts already at $t_{\text{mil}} = 1$ h.

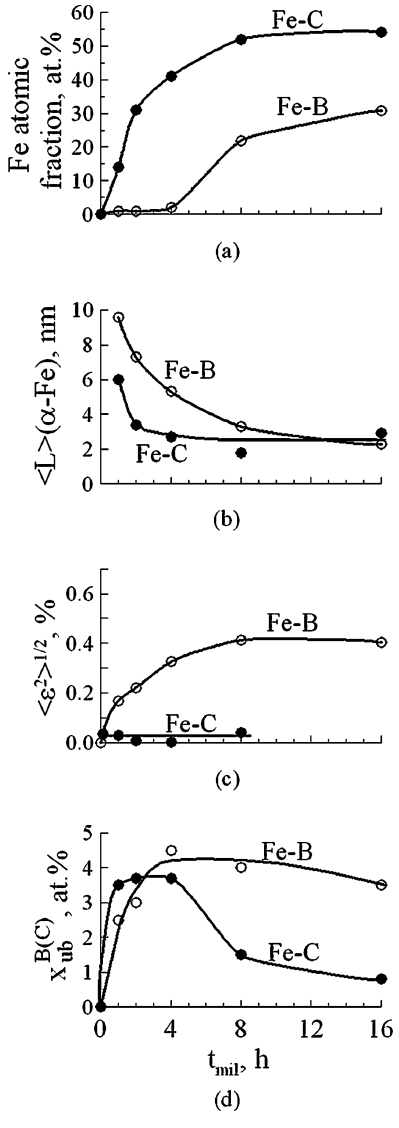

Figure 2 Comparative analysis of MA in Fe(85)C(15) [11] and Fe(85)B(15) (present work) mixtures: Fe atomic fraction in amorphous phase (a), α-Fe grain size ($\langle L \rangle$) (b), α-Fe root mean-squared strain ($\langle \varepsilon^2 \rangle^{1/2}$) (c), C and B amount in segregations on the α-Fe grain boundaries (d).

In the Fe-B system intensive growth of the amorphous phase amount is revealed at $t_{\text{mil}} > 4$ h and the maximum fraction of Fe atoms in it at $t_{\text{mil}} = 16$ h is 30%, i.e. about one half of that in the Fe-C system. The differences in the MA kinetics are revealed in the rate of the grain size decrease (Fig. 2b) and in the level of microstrains (Fig. 2c).

What is the reason of differences in kinetics of SSRs? Consider the kinetics of penetration and segregation of C and B atoms in the grain boundaries of α-Fe. For this purpose it is necessary to estimate what amount of B and C out of initial 15 at.% is chemically bound with the Fe atoms in the amorphous phase after MA (x^{B}_{Am} and x^{C}_{Am}) and after the annealing following the MA (x^{B}_{400} and x^{C}_{500}) in borides and carbides correspondingly (the subscripts indicate the annealing temperatures). The values of x^{C}_{Am} and x^{B}_{Am} can be found according to the known average values of HFMF $\bar{\text{H}}$ for the amorphous Fe-C and Fe-B alloys [24, 31] and from the known fraction of the Fe atoms in the amorphous phase (Fig. 2a). From the distribution functions of HFMF P(H) for the mechanically alloyed samples Fe(85)C(15) and Fe(85)B(15) the values of $\bar{\text{H}}$ were calculated for the part of P(H) function corresponding to the amorphous phase. From [24, 31] we found the maximum values of the C and B concentrations in the amorphous phases 25 and 20 at.%, respectively. Then, the maximum amount of C and B chemically bound with the Fe atoms x^{C}_{Am} and x^{B}_{Am} were calculated. Further procedure was to carry out a low-temperature annealing of the mechanically alloyed samples during 1 h at 500°C for the Fe(85)C(15) and at 400°C for the Fe(85)B(15). First, it was established that annealing at these temperatures of initial mixtures without mechanical treatment does not result in formation of any phases. Annealing of the samples after MA leads to the formation of the Fe_3C carbide in the Fe(85)C(15), $(Fe_2B)'$ and Fe_3B borides in the Fe(85)B(15). $(Fe_2B)'$ boride designated in [25] as x-Fe_2B is a metastable modification of the Fe_2B boride [28, 32]. From the MS of the annealed samples the fractions of the area referring to the carbide and borides were found. Then from the stoichiometric ratios in these phases the total amount of C (x^{C}_{500}) and B (x^{B}_{400}) chemically bound in the carbide and borides was calculated. The values $x^{\text{C}}_{\text{ub}} = x^{\text{C}}_{500} - x^{\text{C}}_{\text{Am}}$ and $x^{\text{B}}_{\text{ub}} = x^{\text{B}}_{400} - x^{\text{B}}_{\text{Am}}$ are the amount of the C and B atoms chemically unbounded with the Fe atoms in α-Fe particles after MA (Fig. 2). The segregations of C and B atoms are at the α-Fe boundaries and they are the source for the amorphous phase formation in the interfaces of the α-Fe nanostructure. This is confirmed by the given above analysis of the Am(Fe-C) amount. From the $x^{\text{C}}_{\text{ub}}(t_{\text{mil}})$ and $x^{\text{B}}_{\text{ub}}(t_{\text{mil}})$ data presented in Fig. 2d, it follows that the kinetics of the segregation formation at MA of the Fe(85)C(15) and Fe(85)B(15) systems coincides both in the time of mechanical treatment and by the amount of B and C in the segregations (~4 at.%). Under these conditions a considerable difference found in the kinetics of the amorphous phase formation (Fig. 2a) can be accounted for by the difference in the covalent radii and, accordingly, by a different penetrating ability of B and C from the segregation into the close-to-boundary distorted zones.

3.3. Mechanical alloying of Fe-Si mixtures

Published data [4, 5, 33–38] infer that the most stable intermetallic compound (ε-FeSi) is formed at the first stage. Up to the concentration of 32 at.% Si [4, 5, 33], the supersaturated solid solution (SSS) is formed at the second stage. The process of MA in the Fe(68)Si(32) and Fe(75)Si(25) mixtures is given in detail in [4, 5]. The quantitative analysis of the MA process in these systems is illustrated in Fig. 3, from which it is seen that:

(i) All SSRs take place on α-Fe reaching the nanocrystalline state;

(ii) The kinetics of SSRs is conditioned by the concentration of Si in the initial mixture;

(iii) The maximum Si concentration in α-Fe(Si) SSS is realized practically simultaneously with its formation.

The amount of the ε-FeSi phase at the first stage of MA can be explained by its formation only in the interfaces of the nanostructure of the α-Fe particles. Using the values of the grain sizes in α-Fe particles $\langle L\rangle = 5.5$ nm (Fe(75)Si(25), $t_{\text{mil}} = 2$ h), $\langle L\rangle = 6.5$ nm (Fe(68)Si(32), $t_{\text{mil}} = 4$ h) and the width of the interfaces $d = 1$ nm, we obtain the volume fractions of the interfaces $f_{\text{if}} = 30$ and 20%, which agree with the maximum amounts of the ε-FeSi phase satisfactorily.

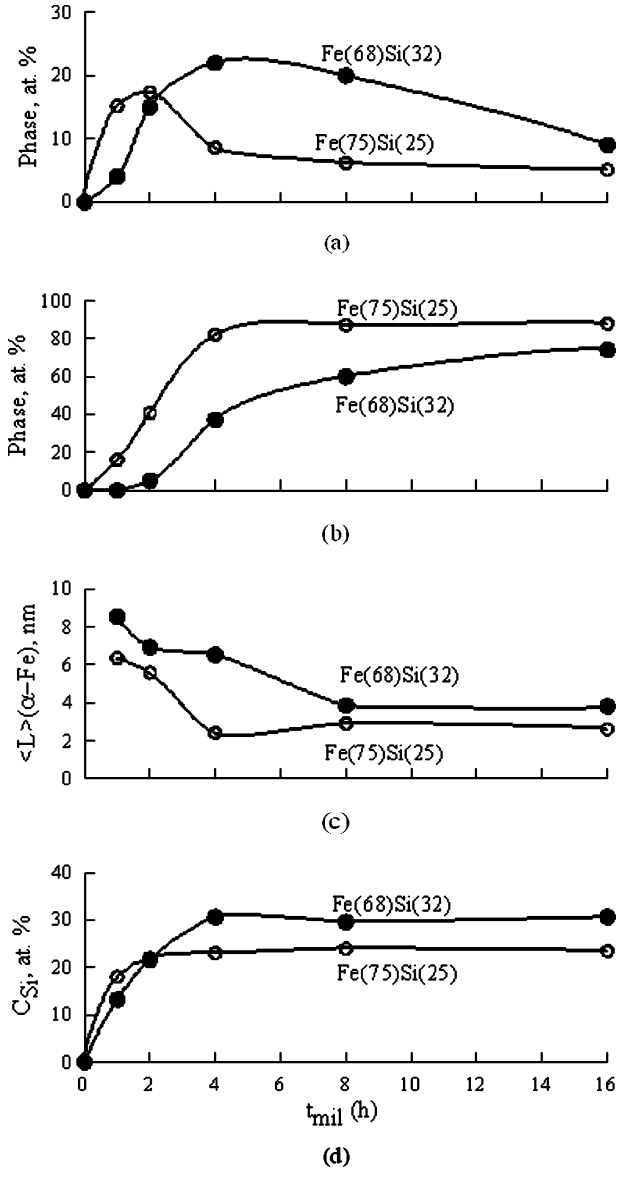

Figure 3 Comparative analysis of MA in Fe(68)Si(32) [4] and Fe(75)Si(25) [5] mixtures: ε-FeSi atomic fraction (a), α-Fe(Si) atomic fraction (b), α-Fe grain size (c) and Si concentration in α-Fe(Si) solid solution (d).

3.4. Comparative analysis of mechanical alloying in the Fe-M systems (M is Si, Ge and Sn isoelectron sp-elements)

The ratio of covalent radii $R_{\text{M}}/R_{\text{Fe}}$ is 0.95, 1.04 and 1.21 for Si, Ge and Sn, respectively. The Fe-Si and Fe-Ge systems have a rather extended range of equilibrium solid solutions, meanwhile the solubility of Sn in α-Fe is low (3.2 at.% at 600°C). The sequence of SSRs in the Fe-Ge and Fe-Sn systems is similar to that in the Fe-Si system. At the first stage, $FeGe_2$ intermetallic in the amorphous or nanocrystalline modifications is formed as well as $FeSn_2$, at the second stage—supersaturated solid solutions of Ge and Sn in α-Fe if the Ge and Sn concentration in the initial mixtures does not exceed 32 at.% [1–3, 9, 10, 33, 38–44]. It is of interest to compare the dependences of the phase amount, Si (Ge, Sn) concentrations in SSS and structural parameters for the given systems on the milling time in MA. Fig. 4a and b collect the time dependences of the compounds and SSS amount; Fig. 4c shows the α-Fe grain size dependences $\langle L\rangle(t_{\text{mil}})$. Their comparison shows that all SSRs take place on α-Fe reaching a nanocrystalline state, a less grain size being necessary to form SSS than to form an intermetallic compound. For all the systems an average grain size in SSS of α-Fe(M) is 2–4 nm. In [4, 5, 9] we showed that the amount of the intermetallic formed at the first stage of MA can be explained by its formation in the interface regions of the nanocrystalline α-Fe. Thus, the first stage of MA includes penetration of sp-atoms along the grain boundaries of α-Fe, their segregation at the boundaries and formation of the first Fe-M phases in the interfaces. Formation of the Si, Ge, Sn and Al segregation is considered in detail in Section 3.6.

The sp-element type influences the kinetics. Consider two extreme cases—MA in the Fe-Si and Fe-Sn systems. The $FeSn_2$ is formed and disappears fast, meanwhile the rate of the ε-FeSi formation is slower, and it is present during the whole MA process (Fig. 4a). As for SSS, it is also formed much faster in the Fe-Sn system than in the Fe-Si one (Fig. 4b). However, a different situation takes place in the saturation of solid solutions (Fig. 4d). In the Fe-Si and Fe-Ge systems the maximum Si(Ge) concentration reaches actually simultaneously with the formation of the solid solution, meanwhile in the Fe-Sn system the solid solution is saturated with Sn gradually. Concerning saturation of solid solution with Si, Ge and Sn one can make following supposition.

At present, two possible mechanisms of accelerated diffusion in MA are discussed. There is interstitial diffusion at the collision moment [45] and diffusion along dislocations [46]. Taking into account the ratio of the atomic sizes in the Fe-Si, Fe-Ge and Fe-Sn systems, one can suppose that the accelerated diffusion in the

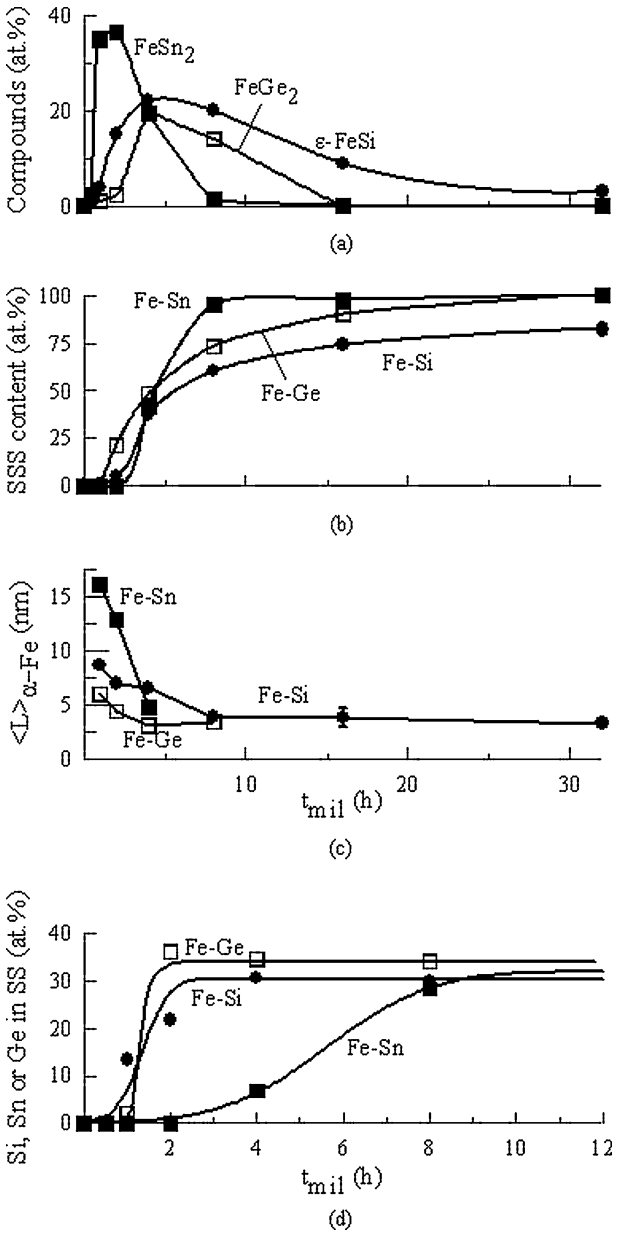

Figure 4 Comparative analysis of MA in Fe(68)M(32); M = Si, Ge and Sn systems [6]: intermetallic compound atomic fraction (a), α-Fe(M) atomic fraction (b), α-Fe grain size (c) and M concentration in α-Fe(M) solid solution (d).

Fe-Si and Fe-Ge systems proceeds mainly along interstices, but in the Fe-Sn system dislocation transfer takes place. Since the density of interstices is always higher than that of dislocations, the saturation rate of the solid solution in the Fe-Si system should be higher than in the Fe-Sn system. However, it is known [15] that with the grain size $\langle L \rangle < 10$ nm there are no dislocations in the grain bulk. We consider the dislocation transfer as generation of dislocations at the moment of impact, their passing through the grain body and leaving for the boundary. Such a process can provide the penetration of the second component (Sn) into the grain bulk of α-Fe.

3.5. Comparative analysis of MA in the Fe-Al and Fe-Si systems

The Al and Si atoms have the sizes close to the Fe atom: $R_{Si}/R_{Fe} = 0.95$ and $R_{Al}/R_{Fe} = 1.01$. Equilibrium phase diagrams are characterized by the extended concentration range of solid solutions. The most important differences are the electron configuration of external shell of atoms, structure, melting temperature and mechanical properties of pure elements. MA in the Fe-Al system with the Al content in the initial mixtures x from 10 to 90 at.% has been intensively studied for the past 15 years [33, 47–67]. In most detail the type and mechanisms of SSRs were investigated for the mixtures with $x \geq 50$ at.% Al [47–53, 55, 56] and close to the stoichiometric composition Fe(75)Al(25) [33, 52, 54, 56, 58, 64, 67]. The analysis of the published results leads to the following conclusions:

(i) MA takes place in the conditions on reaching the nanostructure state ($\langle L \rangle \leq 10$ nm);

(ii) At the first stage of MA a phase is formed, which is revealed in the MS as a paramagnetic doublet at room temperature [48–50, 53, 55, 58, 64, 66]. With $x = 75$–80 at.% Al this phase is a final product of MA and is in the amorphous state [47–50, 53, 59, 60]. With $x \leq 50$ at.% Al it is found in the MS. In [53, 63, 64] it is supposed that this phase is due to the Fe diffusion into Al. The phase contains 70–80 at.% of Al, as in annealing it is transformed into intermetallic Fe_2Al_5 [51, 52, 56, 60, 61]. Further this phase will be referred to as Am(Fe_2Al_5);

(iii) It is established that the formation of the SSS α-Fe(Al) as a final product of MA takes place with $x \leq 60$ at.% Al though in a number of papers the formation of SSS was found with $x = 75$ at.% Al [55–57];

(iv) It was shown [58, 64] that the composition of SSS from the beginning of its formation is close to that of the initial mixture;

(v) Comparative study of the mechanisms and kinetics of SSRs in the Fe-Al and Fe-Si systems with equal compositions of initial mixtures and conditions of mechanical treatment has not been carried out yet.

To compare the processes of MA in the Fe-Si and Fe-Al systems in the present work the composition Fe(68)Al(32) has been chosen. The XRD and MS data for mechanically alloyed samples Fe(68)Al(32) on the whole agree with the given above results of the published papers. However, in contrast to [53, 63, 64] we have not found any changes of the fcc lattice parameter of Al, that would point to the Fe solubility in Al. The amount of the phases formed, the α-Fe grain size and Al concentration in SSS α-Fe(Al) calculated from the XRD and Mössbauer data are presented in Fig. 5. The latter was calculated according to [68, 69] from the values of the bcc lattice parameter and average values of HFMF for α-Fe(Al) SSS. The amount of the Am(Fe_2Al_5) phase can be accounted for its formation in the α-Fe particles interfaces. Under the given values of the undistorted part of the grain of α-Fe $\langle L \rangle = 7$ nm ($t_{mil} = 2$ h) and $d = 1$ nm we obtained the volume fraction of the interfaces $f_{if} = 23\%$, correlating with the atomic fraction of this phase 29% (Fig. 5a). In Fig. 5

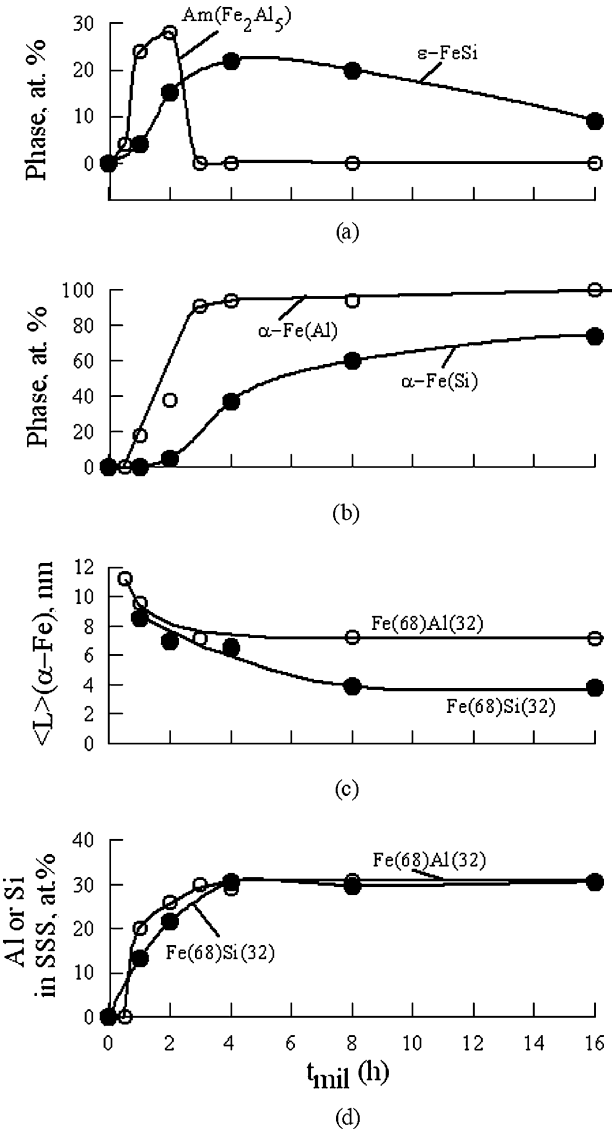

Figure 5 Comparative analysis of MA in Fe(68)Si(32) [6] and Fe(68)Al(32) (present work) mixtures: intermetallic compound atomic fraction (a), α-Fe(Si) atomic fraction (b), α-Fe grain size (c) and Si(Al) concentration in α-Fe(Si, Al) solid solution (d).

the data for the Fe(68)Si(32) system are also presented. Comparing the results, we arrive at the conclusion that with a similar character of SSRs the kinetics of the phase formation in the Fe-Al and Fe-Si systems is substantially different. The amorphous phase $Am(Fe_2Al_5)$ forms and disappears more quickly in comparison with the ε-FeSi phase (Fig. 5a). The rate of SSS formation in the Fe-Al also exceeds that of the Fe-Si (Fig. 5b), despite the fact that $\langle L\rangle_{\alpha\text{-Fe(Al)}} > \langle L\rangle_{\alpha\text{-Fe(Si)}}$ (Fig. 5c). However, the kinetics of saturation of the SSS with Al and Si is practically similar (Fig. 5d), which testifies to the interstitial character of the Al diffusion into the α-Fe grain under pulse mechanical treatment. The kinetics of the phase formation can be influenced by both individual properties of pure materials (mechanical properties, melting temperature, etc.) and atomic characteristics of sp-elements (atomic size and configuration of the external electron shell). To find out the main reason, consider the process of formation of Al, Si, Ge and Sn segregations at the initial stage of MA.

3.6. Al, Si, Ge and Sn segregation at the grain boundaries of the α-Fe nanostructure

The possibility of segregation of Al, Si, Ge and Sn atoms in the α-Fe particles in MA follows from the early disappearance of reflections from pure sp-elements in the XRD. Fig. 6a presents the dependences of the amounts of pure elements Fe, Al, Si, Ge and Sn on the milling time, obtained from XRD. The increase of the α-Fe amount at low values of t_{mil} points either to sp-atoms leaving the coherent scattering regions, or to decreasing pure sp-element due to their interaction with the walls of the vial and balls, or due to the appearance of the vial and balls (hardened steel) material in the samples because of wear. In [10, 11] we showed for the Fe(50)Ge(50) mixture that the increase of the α-Fe amount according to the data of XRD can be explained only by the Ge atoms leaving the coherent scattering regions for the grain boundaries of α-Fe and their segregation at them as the chemical analysis showed the composition 50:50 in the mechanically alloyed samples, and no changes were found out in the masses of the sample, vial and balls before and after milling. The latter also holds for all the systems of Fe-M at $t_{mil} \leq 8$ h. Write the amount of atoms of sp-elements in the segregated state in the α-Fe particles, $x_{ub}(t_{mil})$, as: $x_{ub}(t_{mil}) = x(0) - [x(t_{mil}) + x_{IC}(t_{mil}) + x_{SSS}(t_{mil})]$, where $x(0)$ and $x(t_{mil})$ are the amount of sp-elements in the initial mixture and with the given value of t_{mil}

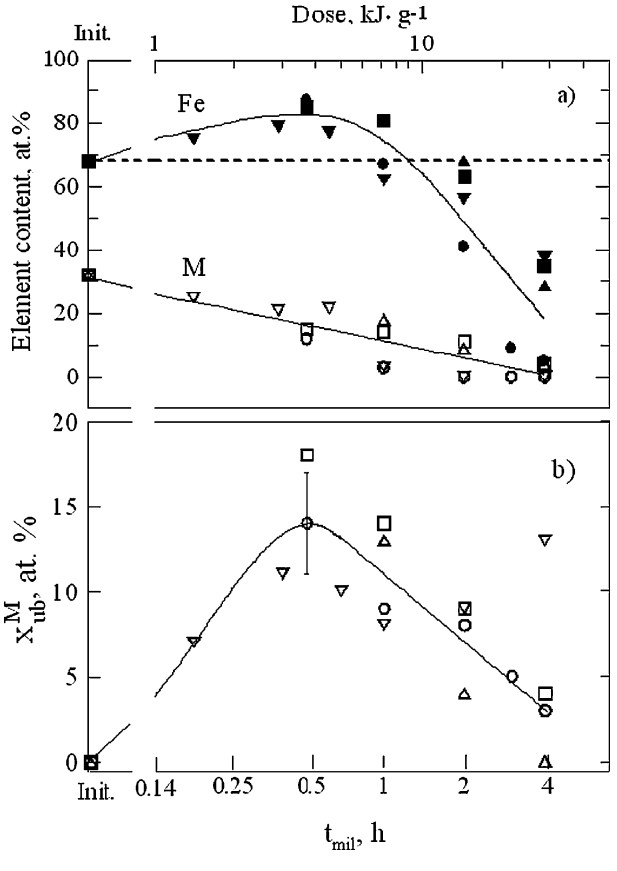

Figure 6 Contents of pure Fe (closed symbols) and M (open symbols) elements according to XRD data (a) and calculated M-element amount (x^M_{ub}) in segregation against milling time (dose loaded mechanical energy) (b). M = Al (○), Si (□), Ge (△), Sn (▽).

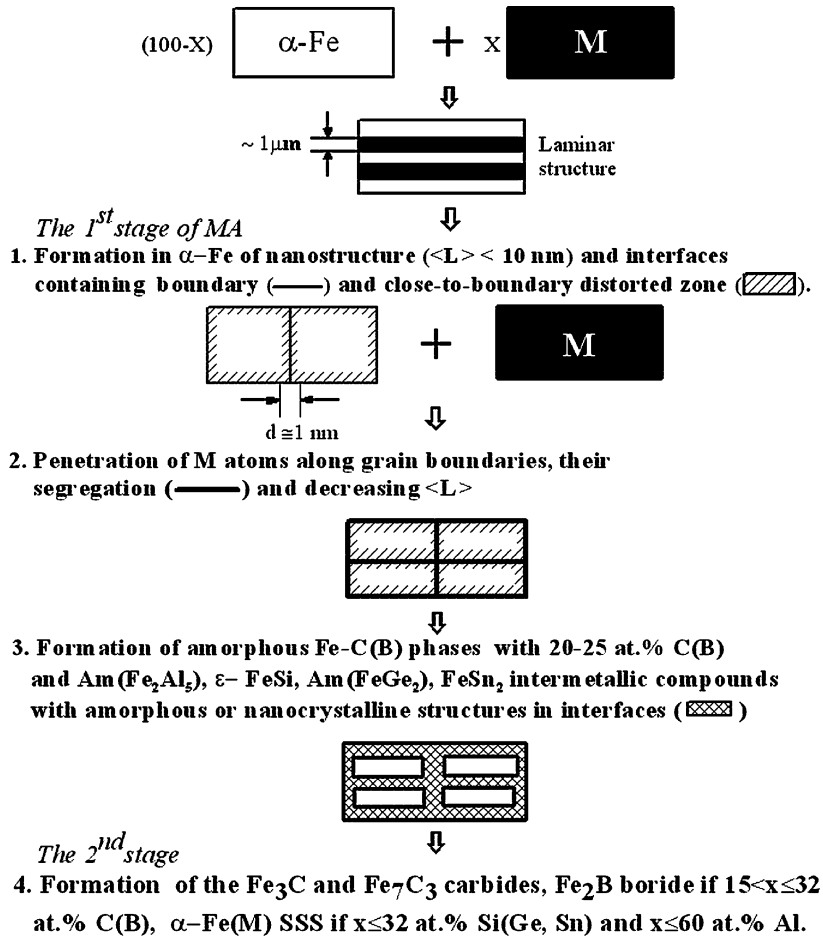

Figure 7 Microscopic model of mechanical alloying of Fe with sp-element (M); M = B, C, Al, Si, Ge and Sn.

according to the data of XRD, $x_{IC}(t_{mil})$ and $x_{SSS}(t_{mil})$ are the concentrations of sp-atoms, chemically bound with the Fe atoms in the intermetallic compound and supersaturated solid solution, determined by both the data of XRD and MS. The calculated values of x_{ub} for Al, Si, Ge and Sn are given in Fig. 6b, from which it is seen that independently of individual properties of pure materials the kinetics of segregations formation at $t_{mil} \leq 2$ h is similar. It means that individual characteristics of sp-atoms affect the kinetics of the phase formation. Retaining a large amount of segregated Sn atoms at $t_{mil} = 4$ h is a consequence of slow saturation of SSS with Sn, having a large covalent radius. Taking into account the segregation of sp-atoms at the grain boundaries of α-Fe, we have shown in the thermodynamic calculations the energy gain of SSS formation when the grain size becomes lower than some critical one [3]. Besides, the presence of segregations allows to understand the phase formation in the interfaces of the α-Fe particles at the first stage of MA.

4. Conclusion

Common and distinctive features of mechanical alloying of Fe with sp-elements have been considered. The common regularities are following: the formation of a nanostructural state in α-Fe particles, sp-atoms penetration along the α-Fe grain boundaries, their segregation and the first Fe-M phase formation in the interfaces (boundary and close-to-boundary distorted zones) at the initial stage; the realization of any type of SSRs only on reaching the nanocrystalline state. The differences in the type of SSRs and their kinetics are conditioned by the ratio of the covalent radii, external shell electron configuration of sp-atom and sp-element concentration (x) in the initial mixture. In alloying α-Fe with sp-elements (Al, Si, Ge, Sn) having approximately equal and substantially larger atomic size, intermetallic compounds are formed in interfaces at the first stage. At the final stage supersaturated solid solution (SSS) is formed in the grain bulk if $x \leq 32$ at.% Si (Ge, Sn) and ≤ 60 at.% Al. In the Fe-Al (Si, Ge) systems the sp-element concentration in SSS becomes maximum simultaneously with the SSS formation, while in the Fe-Sn system SSS is saturated with Sn gradually. In α-Fe alloying with the C and B atoms of a small radius an amorphous phase (Am(Fe-M)) is formed in interfaces at the initial stage. The Am(Fe-B) formation is characterized by a substantially slower kinetics in comparison with that of the Am(Fe-C) one. If $x > 15$ at.% C(B) the second stage—the carbide and boride formation—takes place after amorphization. According to the results published by other authors and obtained in our studies we suggest the scheme of mechanical alloying of Fe with sp-element (M), M = B, C, Al, Si, Ge and Sn shown in Fig. 7.

Acknowledgments

The authors express their gratitude to Prof. V. V. Boldyrev, Dr. T. F. Grigoryeva, Dr. G. N. Konygin, Dr. A. L. Ulyanov, Dr. V. A. Barinov and Dr. V. A. Zagainov for collaboration.

This work has been supported by the Russian Fund for Basic Research (projects 97-03-33483 and 00-03-32555).

References

1. E. P. YELSUKOV, G. A. DOROFEEV, V. A. BARINOV, T. F. GRIGOR'EVA and V. V. BOLDYREV, *Mater. Sci. Forum* **269–272** (1998) 151.
2. G. A. DOROFEEV, G. N. KONYGIN, E. P. YELSUKOV, I. V. POVSTUGAR, A. N. STRELETSKII, P. YU. BUTYAGIN, A. L. ULYANOV and E. V. VORONINA, in "Mössbauer Spectroscopy in Materials Science," edited by M. Miglierini and D. Petridis (Kluwer Academic Publishers, The Netherlands, 1999) p. 151.
3. G. A. DOROFEEV, E. P. YELSUKOV, A. L. ULYANOV and G. N. KONYGIN, *Mater. Sci. Forum* **343–346** (2000) 585.
4. G. A. DOROFEEV, A. L. ULYANOV, G. N. KONYGIN and E. P. ELSUKOV, *Phys. Met. Metallogr.* **91** (2001) 47.
5. E. P. ELSUKOV, G. A. DOROFEEV, G. N. KONYGIN, V. M. FOMIN and A. V. ZAGAINOV, *ibid.* **93** (2002) 93.
6. E. P. YELSUKOV and G. A. DOROFEEV, *Chem. Sustain. Develop.* **1** (2002) 243.
7. E. P. ELSUKOV, G. A. DOROFEEV, V. M. FOMIN, G. N. KONYGIN, A. V. ZAGAINOV and A. N. MARATKANOVA, *Phys. Met. Metallogr.* **94** (2002) 43.
8. E. P. YELSUKOV, G. A. DOROFEEV and V. M. FOMIN, *J. Metastable Nanocryst. Mater.* **15/16** (2003) 445.
9. E. P. ELSUKOV, G. A. DOROFEEV, A. L. ULYANOV, O. M. NEMTSOVA and V. E. PORSEV, *Phys. Met. Metallogr.* **95** (2003) 60.
10. E. P. ELSUKOV, G. A. DOROFEEV, A. L. ULYANOV and A. V. ZAGAINOV, *ibid.* **95** (2003) 486.
11. E. P. YELSUKOV, G. A. DOROFEEV and V. V. BOLDYREV, *Doklady Chimii* **391** (2003) 206.
12. T. TANAKA, S. NASU, K. N. ISHIHARA and P. H. SHINGU, *J. Less-Comm. Met.* **171** (1991) 237.
13. C. SURYANARAYANA, *Progr. Mater. Sci.* **46** (2001) 1.
14. E. P. ELSUKOV, G. A. DOROFEEV, A. L. ULYANOV, A. V. ZAGAINOV and A. N. MARATKANOVA, *Phys. Met. Metallogr.* **91** (2001) 46.
15. M. L. TRUDEAU and R. SCHULZ, *Mater. Sci. Eng.* A **134** (1991) 1361.
16. Z. HORITA, D. J. SMITH, M. FURAKAWA, M. NEMOTO, R. Z. VALIEV and T. G. LANGDON, *Mater. Characteriz.* **37** (1996) 285.
17. G. LE CAËR and P. MATTEAZZI, *Hyperfine Interactions* **66** (1991) 309.
18. G. M. WANG, A. CALKA, S. J. CAMPBELL and W. A. KACZMAREK, *Mater. Sci. Forum* **179–181** (1995) 201.
19. S. J. CAMPBELL, G. M. WANG, A. CALKA and W. A. KACZMAREK, *Mater. Sci. Eng.* A **226–228** (1997) 75.
20. G. LE CAËR, E. BAUER-GROSSE, A. PIANELLY, E. BOUZY and P. MATTEAZZI, *J. Mater. Sci.* **25** (1990) 4726.
21. K. TOKUMITZU, *Mater. Sci. Forum* **235–238** (1997) 127.
22. K. TOKUMITZU and M. UMEMOTO, *ibid.* **360–362** (2001) 183.
23. V. M. NADUTOV, V. M. GARAMUS and J. C. RAWERS, *ibid.* **343–346** (2000) 721.
24. E. BAUER-GROSSE and G. LE CAËR, *Phys. Mag.* B **56** (1987) 485.
25. H. OKUMURA, K. N. ISHIHARA, P. H. SHINGU and H. S. PARK, *J. Mater. Sci.* **27** (1993) 153.
26. A. CALKA, A. P. RADLINSKI and R. SHANKS, *Mater. Sci. Eng.* A **133** (1991) 555.
27. J. JING, A. CALKA and S. J. CAMPBELL, *J. Phys.: Condens. Matter* **3** (1991) 7413.
28. V. A. BARINOV, V. A. TSURIN, E. P. ELSUKOV, L. V. OVECHKIN, G. A. DOROFEEV and A. E. ERMAKOV, *Phys. Met. Metallogr.* **74** (1992) 412.
29. J. BALOGH, T. KEMENY, I. VINCZE, L. BUJDOSO, L. TOTH and G. VINCZE, *J. Appl. Phys.* **77** (1995) 4997.
30. E. C. PASSAMANI, J. R. B. TAGARRO, C. LARIKA and A. A. R. FERNANDES, *J. Phys.: Condens. Matter* **14** (2002) 1975.
31. C. L. CHIEN, D. MUSSER, E. M. GYORGY, R. C. SHERWOOD, H. S. CHEN, F. E. LUBORSKY and J. L. WALTER, *Phys. Rev.* B **20** (1979) 283.
32. V. A. BARINOV, G. A. DOROFEEV, L. V. OVECHKIN, E. P. ELSUKOV and A. E. ERMAKOV, *Phys. Met. Metallogr.* **73** (1992) 93.
33. C. BANSAL, Z. Q. GAO, L. B. HONG and B. FULTZ, *J. Appl. Phys.* **76** (1994) 5961.
34. E. GAFFET, N. MALHOUROUX and M. ABDELLAOUI, *J. Alloys Compd.* **194** (1993) 339.
35. M. ABDELLAOUI, T. BARRADI and E. GAFFET, *ibid.* **198** (1993) 155.
36. M. ABDELLAOUI, E. GAFFET and C. DJEGA-MARIADASSOU, *Mater. Sci. Forum* **179–181** (1995) 109.
37. N. ŠTEVULOVÁ, A. BUCHAL, P. PETROVIČ, K. TKÁČOVÁ and V. ŠEPELÁK, *J. Magn. Magn. Mater.* **203** (1999) 190.
38. A. F. CABRERA, F. H. SANCHEZ and MENDOZA-ZELIS, *Mater. Sci. Forum* **312–314** (1999) 85.
39. S. SARKAR, C. BANSAL and A. CHATTERJEE, *Phys. Rev.* B **62** (2000) 3218.
40. A. F. CABRERA and F. H. SANCHEZ, *ibid.* **65** (2002) 094202–1.
41. S. NASU, P. H. SHINGU, K. N. ISHIHARA and F. E. FUJITA, *Hyperfine Interactions* **55** (1990) 1043.
42. S. NASU, S. IMAOKA, S. MORIMOTO, H. TANIMOTO, B. HUANG, T. TANAKA, J. KUJAMA, K. N. ISHIHARA and P. H. SHUGU, *Mater. Sci. Forum* **88–90** (1992) 569.
43. G. LE CAËR, P. DELCROIX, M. O. KIENTZ and B. MALAMAN, *ibid.* **179–181** (1995) 469.
44. M. O. KIENTZ, G. LE CAËR, P. DELCROIX, L. FOURNES, B. FULTZ, P. MATTEAZI and B. MALAMAN, *Nanostruct. Mater.* **6** (1995) 617.
45. P. YU. BUTYAGIN, *Chem. Rev.* B **23**, (Part 2) (1998) 89.
46. R. B. SCHWARZ, *Mater. Sci. Forum* **269–272** (1998) 663.
47. P. H. SHINGU, B. HUANG, J. KUYAMA, K. N. ISHIHARA and N. NASU, in "New Materials by Mechanical Alloying Techniques," edited by E. Artz and L. Schultz (DGM Informationgeselschaft, Oberursel, 1989) p. 319.
48. W. H. WANG, K. Q. XIAO, Y. D. DONG, Y. Z. HE and G. M. WANG, *J. Non-Cryst. Solids* **124** (1990) 82.
49. G. M. WANG, D. Y. ZHANG, W. H. WANG and Y. D. DONG, *J. Magn. Magn. Mater.* **97** (1991) 73.
50. Y. D. DONG, W. H. WANG, L. LIU, K. Q. XIAO, S. H. TONG and Y. Z. HE, *Mater. Sci. Eng.* A **134** (1991) 867.
51. W. GUO, S. MARTELLI, F. PADELLA, M. MAGINI, N. BURGIO, E. PARADISO and U. FRANZONI, *Mater. Sci. Forum* **89/90** (1992) 139.
52. E. BONETTI, G. SCIPIONE, G. VADRE, G. COCCO, R. FRATTINI and P. P. MACRI, *J. Appl. Phys.* **74** (1993) 2058.
53. V. F. FADEEVA, A. V. LEONOV and L. M. KHODINA, *Mater. Sci. Forum* **179–181** (1995) 397.
54. E. BONETTI, G. SCIPIONE, R. FRATTINI, S. ENZO and L. SCHIFFINI, *J. Appl. Phys.* **79** (1996) 7537.
55. S. ENZO, R. FRATTINI, R. GUPTA, P. P. MACRI, G. PRINCIPI, L. SCHIFFINI and G. SCIPIONE, *Acta Mater.* **43** (1996) 3105.
56. S. ENZO, G. MULAS and R. FRATTINI, *Mater. Sci. Forum* **269–272** (1998) 385.
57. S. ENZO, R. FRATTINI, G. MULAS and F. DELOGU, *ibid.* **269–272** (1998) 391.
58. K. WOLSKI, G. LE CAËR, P. DELCROIX, R. FILLIT, F. THEVENOT and J. LE COZE, *Mater. Sci. Eng. A* **207** (1996) 97.

59. E. JARTYCH, J. K. ZURAWICZ, D. OLESZAK, J. SARZYNSKI and M. BUDZYNSKI, *Hyperfine Interactions* **99** (1996) 389.
60. D. OLESZAK, P. H. SHINGU and H. MATYJA, in "Rapidly Quenched and Metastable Materials," edited by P. Duhaj, P. Mrafko and P. Svec (Elsevier, The Netherlands, 1997) p. 18 (Supplement).
61. D. OLESZAK and P. H. SHINGU, *Mater. Sci. Forum* **235–238** (1997) 91.
62. D. OLESZAK, M. PEKALA, E. JARTYCH and J. K. ZURAWICZ, *ibid.* **269–272** (1998) 643.
63. E. JARTYCH, J. K. ZURAWICZ, D. OLESZAK and M. PEKALA, *J. Phys.: Condens. Matter* **10** (1998) 4929.
64. D. E. EELMAN, J. R. DAHN, G. R. MACKKAY and R. A. DUNLAP, *J. Alloys Compd.* **266** (1998) 234.
65. M. HASHII, *Mater. Sci. Forum* **312–314** (1998) 139.
66. M. HASHII and K. TOKUMITSU, *ibid.* **312–314** (1999) 399.
67. G. GONZALES, L. D'ANGELO, J. OCHOA and L. D'ONOFRIO, *ibid.* **360–362** (2001) 349.
68. E. P. YELSUKOV, E. V. VORONINA and V. A. BARINOV, *J. Magn. Magn. Mater.* **115** (1992) 271.
69. G. A. PEREZ ALCAZAR and B. GALVAO DA SILVA, *J. Phys. F.: Metal. Phys.* **17** (1987) 2323.

Received 11 September 2003
and accepted 27 February 2004